

Introduction to the artificial neural network-based variational Monte Carlo method

William Freitas¹

¹*Max Planck Institute for the Physics of Complex Systems, Noethnitzer Str. 38, 01187 Dresden, Germany*

In this self-contained tutorial, the variational Monte Carlo method with trial wave functions based on artificial neural networks is detailed. Unfolding the historical background we illustrate how machine learning interacts with physics research. The mathematical tools for both, artificial neural networks and variational Monte Carlo, are introduced. We demonstrate, how the algorithm operates with generic examples from chemical physics, including the harmonic, the Morse, the Poschl-Teller and the Yukawa potential, as well as the simplest molecules, the hydrogen molecular ion and the hydrogen molecule.

I. INTRODUCTION

The recent extensive adoption and incorporation of artificial intelligence-based tools in scientific research promoted considerable advancements over several domains, particularly in physics. Extensive amount of applications showed outstanding relevance, covering from cosmology [1] and particle physics [2] up to many-body quantum systems [3], quantum chemistry [4, 5], statistical mechanics [6], and materials [7]. The absorption of artificial neural networks (ANN) and other artificial intelligence (AI) tools in the physics research is natural in some respects. The reason is that those tools are built with the purpose of recognizing patterns in data and acquiring knowledge from the process. In the same way, the recognition of patterns in physical phenomena and their description in mathematical terms is spread throughout the natural sciences, possibly since the forerunner civilizations that studied astronomy. Therefore, employing such tools from the AI field in order to assist our development of knowledge across all domains of science is indeed straightforward.

Variational wave functions have already demonstrated to be exceptionally effective in explaining some phenomena such as superconductivity [8], spin liquids [9], and the quantum Hall effect [10]. Consequently, exploring ANNs aiming to build new trial wave functions is promising for two reasons. Firstly, based on Cybenko's theorem [11], widely known as the universal approximation theorem, ANNs are capable of representing an extensively broad class of functions, which includes those that are under the axioms of quantum mechanics. Secondly, variational quantum states that employ ANNs in their structure have already shown success in the investigation of open quantum systems [12], frustrated quantum magnets [13], spin chains [14], interatomic force estimation [15], excited states of atoms and molecules [16], homogeneous electron gas [17, 18], superfluid systems [19], quantum droplets [20, 21], among others [22].

Therefore, the purpose of this article is to provide a historical overview as a motivation and an introductory tutorial on the artificial neural network-based variational Monte Carlo method (ANVMC). To accomplish that, quantum toy problems will be revisited from the variational method (VM) framework and described by an

ANN as the trial wave function. The multi dimensional integrals associated with this calculation are performed using Monte Carlo integration. Hence, the article is organized as follows: The next section covers selected historical facts that lead humanity from the desire to create AI to using modern ANNs as tools to develop scientific knowledge; the third section describes the necessary theoretical background to apply ANVMC; the fourth section shows the results of applying the method to several quantum systems; and the last section concludes with remarks on this work.

II. HISTORICAL BACKGROUND

The desire to create AI has been spread throughout humanity at least since ancient Greece. Some old legends tell about mythical figures such as Hephaestus, god of artisans, blacksmiths, fire and metallurgy. According to Greek mythology, Pandora, the first mortal woman, was forged by Hephaestus, revealing the existing thoughts of that time about human intelligence created artificially. Moreover, this myth also mentions that virtues such as grace and persuasion were given to Pandora by the gods. The current computers can be seen from a similar aspect, where a sequence of adaptable instructions with a specific purpose, in other words, an algorithm is given to the machine in order to automate a procedure. The programmable essence of computers is alike the virtues offered to Pandora and the aspiration to create computers that think still pondering in society nowadays, as they did in ancient Greece.

However, to reach the current stage of AI technologies, important developments were necessary, both intellectually and in terms of technological innovation. In particular, the beginning of programmable computers was due to the desire to automate numerical calculations. Historically, one of the forerunners of this desire was Galileo Galilei with his mathematical formulation of the natural sciences [23]. By uniting natural sciences and math, a demand for a machine that can calculate arose among scientists. That influenced Pascal in the creation of the addition machine in 1642 and, afterwards, it influenced Leibniz in the invention of the Leibniz wheel in 1673. Pascal's device could sum and

subtract, while Leibniz’s device could also make products and divisions. Later, in the 19th century, those devices supported Charles Babbage on the development of both difference and analytical engines, that are considered prototypes of programmable computers. Contemporaneously and based on Babbage’s work, Ada Lovelace proposed a method represented by a sequence of steps to compute the Bernoulli numbers through the analytical engine [24]. Frequently, this method is referenced as the first algorithm created to be processed by a machine, which made Ada known as the first programmer.

In the following century, World War II had an important influence on the development of such machines, leading to the creation of the Bombe, an electro-mechanical device specially assembled to decipher German messages encrypted by the ENIGMA. Among the most important names in this project were Alan Turing due to the introductory design and Gordon Welchman for a crucial refinement on the project [25]. Simultaneously, Turing also aided the development of the computers Colossus Mark 1 and Colossus Mark 2, designed by Tommy Flowers and influenced by Max Newman’s work [26]. These computers also aimed to decipher other kinds of encrypted messages, however, they were based on thermionic valves to perform operations and were more versatile, they could be programmed using switches and plugs.

Not much later than that, in 1945, the machine regarded as the first fully electronic, general-purpose computer, the ENIAC was completed [27]. It operated in the decimal base, and the design is attributed to John Mauchly and John Eckert. Also, both of them worked together with John von Neumann on the successor of ENIAC, the EDVAC computer, which operated on the binary base and was designed to be a stored-program computer, in other words, the program instruction and data could be stored in an accessible memory [28]. That still is a key feature of modern computers and made programming rather simpler compared with ENIAC, in which one has to program through plugboards and switches.

In this context, perhaps also influenced by the same desires as the ancient Greeks, Alan Turing proposed the imitation game [29], which aims to probe if machines are capable of thinking. However, due to the philosophical nature of the meaning of thinking, the question has to be replaced by a feasible experiment. In that sense, the aim of this experiment becomes to determine if machines can mimic human intelligence. Therefore, the Turing test entails three participants: one human interviewer and two interviewed participants, one of them a human and the other a machine. Then, the interviewer talks separately with each interviewed through text messages. Their aim is to find who is the machine and who is the human. Consequently, the machine will try to mimic the behaviour of the human in the conversation and, hence, deceive the interviewer. If the interviewer mistakes the machine for a human, then this machine is capable of thinking in the Turing test sense.

With the development of large generative models such

as GPT-5 [30] and DeepSeek [31], the Turing test is on the verge of being accomplished in the way it was constructed [32]. Not only that, but many other useful technologies such as augmented and virtual reality [33], autonomous vehicles [34], virtual assistants [35], and digital twins [36] employ AI tools. However, to reach the current AI state-of-the-art technologies, from the 50s to nowadays, several important improvements both intellectually and technologically were necessary.

Regarding the technological advancements, one of the most important factors was the miniaturisation of computer components. From the beginning of commercially available general-purpose computers such as the Ferranti Mark I to current AMD Ryzen Threadripper processors, the size of computers has reduced dramatically. Two important events in this period of time were the release of the first commercially available microprocessor by Intel in 1971 and the IBM personal computers in 1981. At that time, the number of transistors in an integrated circuit was about 10^5 . Even before that, a phenomenon known as Moore’s law [37] was observed. The law states that the number of transistors in an integrated circuit approximately doubles every other year. This tendency of growing in numbers is also supported by the miniaturisation, in other words, they also increase the density to keep the devices at a reasonable size. The trend persists even nowadays, 10^{11} is the current order of transistors in a microchip [38].

On the other hand, and parallel to the technological advancements, theoretical progress in the AI field were also necessary. A pivotal tool in this process is deep learning. However, there were three great “waves” of development for this tool to achieve its current design [39]. The first “wave” is known as **cybernetics** and had its beginning during the 40s, while its peak of popularity was around the end of the 60s. Throughout this period of time, the forerunners of deep learning models were only linear models, as, for example, the neuron of McCulloch-Pitts [40]. This model was able to distinguish between two categories of information. However, in order for the neuron to correctly predict between the two categories, it was necessary to adjust the model parameters manually. A few years later, another linear model known as *perceptron* [41] was proposed, and, by learning from examples, it was capable of determining in which of the two categories the information belonged. Currently, the perceptron is still being broadly used in the context of machine learning and also as components of models in deep learning applications.

The second “wave” of development became historically known as **connectionism** and had its beginning during the 80s. The peak of the wave was around the mid-90s, and several advancements took place in this period of time, with many of them remaining up to nowadays as basic blocks for the construction of modern ANNs. Among the core tools that connectionism popularised, one important contribution was the model called *cognitron* [42], which introduced non-linear ways to process

the data given to the model. Before that, only one basic unit, or neuron, was used to compose most of the models. However, the central idea behind the connectionism was to reach intelligent behaviour through connecting computational units together, inspired by the biological neurons. Therefore, it was at this point in time that the forerunner models of the modern ANNs were proposed.

In this context, the concept of distributed representation [43] emerged. In order to understand this idea, consider a vision system that is capable of recognizing shelves, desks, and chairs, and any of them might be made from wood, metal, or plastic. One way of organizing the neurons of a model to perform the recognition of the possible objects is to assign one neuron for each combination of furniture and material. Another way would be to split the neurons into two layers of three neurons each, where one layer can separate the type of furniture, while the other would classify the material. By connecting densely the two layers, only six neurons would be necessary to perform the recognition in this example. That would be the distributed representation of the model, which reduces the number of neurons to achieve the desired goal. This kind of representation enables the neurons to understand complex concepts in terms of simpler concepts. Another remarkable contribution was the success in employing the back-propagation algorithm [44] to train the models and its popularization. Currently, this algorithm is still one of the core tools when training models.

From 2006 on, the third “wave” begins with one work demonstrating that a specific model can be trained efficiently with a strategy called greedy layer-by-layer pre-training [45]. The following works showed that the same strategy could be used to train other types of models and systematically improve their performance [46]. It was in this wave of works that the term “deep learning” was popularized. Eventually, the advancements of such techniques reached physics in all its several domains, where the first application was in condensed matter physics [47]. More recent applications are mentioned in the introduction.

Although the extensive use of machine learning tools applied to physics is recent, there has been cross-breeding between statistical physics and machine learning since connectionism’s wave [48]. An interesting example is the first-order phase transition that takes place in perceptrons when they are being trained by examples [49]. As the number of examples increases, the model reaches the reference state. Another notable connection between these two fields is the Boltzmann machines, which are known as the inverse Ising problem [50] within the physics literature. In this problem, the task is to determine the coupling parameters between spins based on a dataset of Ising model configurations. Another key aspect that both fields share is a special interest in the optimization problem. Particularly, in the context of quantum mechanics, the minimization of the energy functional, also known as the VM, has a direct analogy with machine learning.

III. THEORY

Variational Monte Carlo method

The VM relies on the variational principle [51], which states that, among any normalizable functions, the expectation value of the Hamiltonian \mathcal{H} is always equal or larger than the ground state (GS) energy. Therefore, given a normalizable trial wave function ψ_θ parametrized by variational parameters θ , the energy functional $E[\theta]$ yields an energy expectation value that is an upper bound for the GS energy, namely

$$E[\theta] = \frac{\int d\mathbf{x} \psi_\theta^*(\mathbf{x}) \mathcal{H} \psi_\theta(\mathbf{x})}{\int d\mathbf{x} |\psi_\theta(\mathbf{x})|^2} \geq E_0. \quad (1)$$

This also means that the expectation value $E[\theta]$ has a global minimum that is larger or equal to the GS energy. Minimizing the energy functional with respect to the parameters identifies the function that provides the best approximation to the GS within the variational family ψ_θ . Moreover, considering the scope of this work, the Hamiltonian will be written simply as the sum of kinetic energy and potential energy $\mathcal{H} = \hat{K} + V(\mathbf{x})$, where $\mathbf{x} = \{q_1, q_2, \dots, q_{ND}\}$ are the coordinates of all system components, N being the number of components, and D the number of spacial dimensions considered.

Several interesting systems can be studied throughout trial wave functions. However, the high dimensionality of the integrals involved in Eq. (1) often makes the analytical computation prohibitive. The variational Monte Carlo (VMC) method is the key to overcome this limitation. The formulation of the method requires to rewrite the energy expectation value in terms of the probability density function (PDF) $p(\mathbf{x}) = |\psi_\theta(\mathbf{x})|^2 / \mathcal{N}$, where the normalization factor is given by $\mathcal{N} = \int d\mathbf{x} |\psi_\theta(\mathbf{x})|^2$, and in terms of the local energy function, which is written as $E_L(\mathbf{x}) = \psi_\theta^{-1}(\mathbf{x}) \mathcal{H} \psi_\theta(\mathbf{x})$. By doing so, the energy expectation value reads

$$E[\theta] = \frac{\int d\mathbf{x} |\psi_\theta(\mathbf{x})|^2 \frac{\mathcal{H} \psi_\theta(\mathbf{x})}{\psi_\theta(\mathbf{x})}}{\int d\mathbf{x} |\psi_\theta(\mathbf{x})|^2} = \int d\mathbf{x} p(\mathbf{x}) E_L(\mathbf{x}). \quad (2)$$

In principle, since $p(\mathbf{x})$ is a PDF, the integral can be viewed as a continuous weighted sum of the local energy over the configuration space. However, by drawing a set of M samples $\{\mathbf{x}_i\}_{i=1}^M$ distributed according to $p(\mathbf{x})$, then, the integral could be estimated as a simple average $E_{\text{VMC}} \simeq \sum_{i=1}^M E_L(\mathbf{x}_i) / M$, which converges to the exact value in the limit of large M , with a statistical error that scales as $1/\sqrt{M}$. That procedure is called Monte Carlo integration.

Nevertheless, exactly sampling $p(\mathbf{x})$ can be as hard as solving the full Schroedinger equation. Therefore, a frequent approach when performing a Monte Carlo integration is to employ the Metropolis algorithm [52].

This algorithm is an advanced sampling method that uses rejection techniques, in other words, it involves explicitly proposing tentative values and accepting or rejecting based upon some rules. The method is also iterative in the sense that it utilizes the current values to propose trial ones. The procedure is summarized as follows:

- i chose an initial configuration \mathbf{x}_0 and set $j = 0$;
- ii propose a trial move according to $\mathbf{x}_t = \mathbf{x}_j + \Delta(1/2 - \boldsymbol{\xi})$;
- iii compute the density probability ratio $q = p(\mathbf{x}_t)/p(\mathbf{x}_j)$;
- iv if $q > \xi'$ accept the trial move $\mathbf{x}_{j+1} = \mathbf{x}_t$ or else reject it $\mathbf{x}_{j+1} = \mathbf{x}_j$;
- v set $j = j + 1$ and return to step ii).

Note that the acceptance probability $q = |\psi_\theta(\mathbf{x}_t)|^2/|\psi_\theta(\mathbf{x}_j)|^2$ and, therefore, the procedure does not depend on the normalization \mathcal{N} . Moreover, $\boldsymbol{\xi}$ and ξ' denote, respectively, a ND -dimensional vector and a scalar drawn from a uniform distribution on the interval $[0, 1)$. Generating pseudo random numbers uniformly distributed is a field of its own, where pseudo random number generators such as SPRNG [53] and JAX [54] are examples of efficient generators. Lastly, the step size Δ controls the acceptance ratio, that is, how many moves are accepted among a certain number of steps. The acceptance is large for small step sizes, while the opposite behaviour happens when the step size is large. For the described version of the Metropolis algorithm, the most efficient acceptance rate requires adjusting the step size in order to reach 50% acceptance.

In this work, the initial configurations are chosen randomly. It is important to point out that the initial steps are highly correlated to the initial configurations and, hence, are not sampled according to $p(\mathbf{x})$. Therefore, the energy estimation cannot be trusted in those steps. Nevertheless, after the initial steps, that should be discarded, the procedure converges towards the equilibrium, namely, to the correct distribution. Then, the energy estimation is performed using the correctly sampled configurations as described before. Since this method is stochastic and subsequent steps are correlated, the unbiased estimator of the standard error of the mean (SEM) together with the blocking procedure is necessary in order to evaluate the statistical error present in the estimated result. More details can be found on Appendix A.

Finally, aiming to minimize the energy functional $E[\theta]$, the gradient with respect to the variational parameters is required. By carefully computing the gradient of the ratio present in Eq. (1) and assuming the trial wave function is real, the expression reads

$$\nabla_\theta E[\theta] = \int d\mathbf{x} p(\mathbf{x}) \left(E_L(\mathbf{x}) - \int d\mathbf{x}' p(\mathbf{x}') E_L(\mathbf{x}') \right) \nabla_\theta \ln |\psi_\theta(\mathbf{x})|^2. \quad (3)$$

Employing the same techniques as before, the estimation of this integral is also done through Monte Carlo integration. Accordingly, the gradient is estimated by the average $\nabla_\theta E \simeq M^{-1} \sum_{i=1}^M [E_L(\mathbf{x}_i) - E_{\text{VMC}}] \nabla_\theta \ln |\psi_\theta(\mathbf{x}_i)|^2$, where \mathbf{x}_i are the same configurations sampled from $p(\mathbf{x})$ used to estimate E_{VMC} . Once these quantities are estimated, minimization methods such as the gradient descent might be applied in order to find the minimum of the energy functional and, consequently, the best approximation for the GS within the class of trial functions ψ_θ .

Regression problem in machine learning

The machine learning field is dedicated to the development of algorithms and statistical models that allow the computer to perform tasks without being explicitly programmed. As a practical example, suppose that the task is to correctly predict house prices based on its features, such as size, construction date, electrical system, number of rooms, place, among other quantities. Therefore, the task can be seen as a function that returns the price of the house and it depends on variables that are the features of a given house. Hence, machine learning algorithms have a generic objective to recognize patterns in data and learn from it. Nevertheless, learning is a subjective concept that can be interpreted in several ways. For this reason, the following definition by Mitchell [55] is considered: given an experience E with respect to a class of tasks T and one performance measure P , the concept of learning consists in improving the performance P in the tasks T with experience E .

In the house pricing problem, the task is to predict correctly the price of the houses, the experience is a data set that contains features and price of several houses. How good is the prediction made from the algorithm is the performance. After some training, the algorithm identifies the pattern in the data and improves its performance and, therefore, it learns how to predict a house price outside of the data set. This class of problems is one of the simplest machine learning problems and it is called regression. Usually, the data set can be split into the input features $\mathbf{h}_0^{(i)}$, in other words, the variables relevant for a given task, and their corresponding targets y_i , which are the correct prediction values. The functions used to construct machine learning algorithms are called models. Particularly, an ANN can be used as a model. ANNs can be understood as flexible mathematical functions that are parametrized and constructed aiming to capture complex relations between inputs (variables or features) and outputs (targets).

Hence, consider a parametrized model ϕ_θ that depends on a set of parameters θ . One possible measure of performance for this model is the mean squared error (MSE) over the known data set, which is given by the loss function:

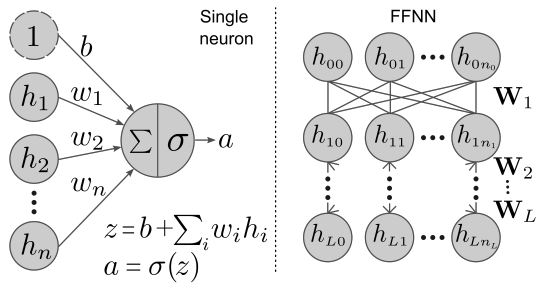


FIG. 1. Schematic representations of a artificial neuron (left) and a FFNN (right).

$$\mathcal{L} = \frac{1}{M} \sum_i \left[\phi_\theta \left(\mathbf{h}_0^{(i)} \right) - y_i \right]^2, \quad (4)$$

where M is the number of samples contained in the data set. In this case, the performance increases as the loss decreases, which means that to achieve the best performance, one has to minimize the loss. There are many ways to construct ANNs for machine learning algorithms and each specific class of tasks usually requires different architectures, that is, different forms of building the model. However, most of them are constructed based on the same basic units, which are called neurons. Mathematically, these units performs an linear transformation followed by a nonlinear transformation of the inputs. Suppose the inputs are given by a vector \mathbf{h} , the linear transformation is given by $z = \mathbf{w}^\top \cdot \mathbf{h} + b$, where \mathbf{w} is a vector of parameters called weights and b is also a parameter called bias. Then, the nonlinear transformation is given by $a = \sigma(z)$, where the nonlinear function σ is referred as activation function. Examples of activation functions are sigmoid, step function, and softplus. For this work, the activation function considered is the hyperbolic tangent unless otherwise stated. An schematic representation of a neuron is illustrated in Fig. 1.

In practice, the neurons are grouped in layers, which takes an input vector and perform the same two transformations, producing an output vector. In other words, if a layer has m neurons and the input vector has dimension n , then the layer is described by a matrix of weights $\mathbf{W} \in \mathbb{R}^{m \times n}$ and a vector of biases $\mathbf{b} \in \mathbb{R}^m$ that performs the linear transformation $\mathbf{z} = \mathbf{W} \cdot \mathbf{h} + \mathbf{b}$, where \cdot indicates a matrix multiplication. Finally, the output vector is denoted by $\mathbf{a} = \sigma(\mathbf{z})$, where the activation function is applied element-wise to each component of \mathbf{z} . One of the simplest architecture of ANNs is the feed-forward neural network (FFNN), which is obtained by stacking several such layers one after another, where the output of one layer becomes the input of the subsequent one. An schematic representation is also included in Fig. 1, where h_{ij} is the j -th component of \mathbf{h}_i , which is the output of the i -th layer, n_i is the number of neurons for the i -th layer, and L is the total number of layers.

Hence, as an educational example, consider the following model built from this mentioned composition of layers and that is limited to predict results in the interval $[0, 1]$

$$\phi(\mathbf{h}_0) = \frac{1}{1 + e^{\mathbf{z}_L}}. \quad (5)$$

Since this function will represent quantum states in the applications considered, this restriction is reasonable. Moreover, the outputs of the final layer L denoted by \mathbf{z}_L are computed using the recurrence relation given by

$$\mathbf{z}_\ell = \mathbf{W}_\ell \cdot \mathbf{h}_{\ell-1} + \mathbf{b}_\ell, \quad (6a)$$

$$\mathbf{h}_\ell = \sigma(\mathbf{z}_\ell), \quad (6b)$$

where \mathbf{W}_ℓ and \mathbf{b}_ℓ are the weights and biases of the ℓ -th layer, while \mathbf{h}_0 is the input features relevant for the task, that is, the input variables for the parametrized function ϕ . Also, $\ell \in \{1, \dots, L\}$ is an index denoting the layer of the ANN and $\theta = \{\mathbf{W}_1, \dots, \mathbf{W}_L\} \cup \{\mathbf{b}_1, \dots, \mathbf{b}_L\}$ contains all parameters of the model. Lastly, utilizing an optimization algorithm, it is possible to find the values of the parameters θ that minimizes the loss function of Eq. (4). Commonly, these algorithms are iterative, which means that the loss value reduces each step that the algorithm is performed until it reaches a minimum and, therefore, the algorithm learns in the sense defined before, since its performance increases as it has more experience.

Moreover, the optimization algorithms frequently rely on gradient based methods. That is natural, since the gradient of any function gives the direction of largest growth rate at the evaluated point. Therefore, the opposite direction can be used as a guide to know how to update the parameters in order to reduce the MSE. Furthermore, computing the gradient of an ANN with respect to the weights and biases usually employs the back-propagation algorithm [44], which is a efficient way of computing derivatives specifically for ANNs. Since the code used in this work utilize automatic differentiation [54], the details of this algorithm are omitted. Finally, the simplest way is the gradient descent that updates the parameters according to

$$\theta_{t+1} = \theta_t - \eta \nabla_\theta \mathcal{L}[\theta_t], \quad (7)$$

where η is the learning rate, a small real number that can be adjusted in order to provide the fastest learning per iteration possible, in other words, the value of η is empirically chosen. Nevertheless, this approach is humble and often not a good option for ANNs. The approach employed in this work is the adaptive moment estimation (ADAM) [56] optimizer, which is described in more details on Section B.

The similarities between ML regression and VM are considerable. Furthermore, it is possible to make a direct connection of each component of their respective methods, as it is represented in Fig. 2. In particular, both can

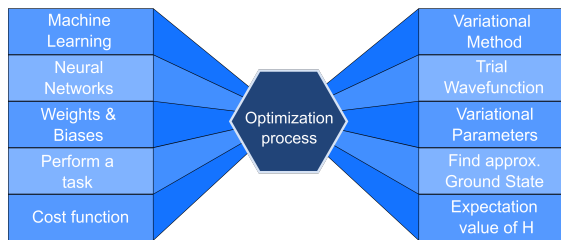


FIG. 2. Analogies between the variational method and machine learning regression showing the equivalent components in each method.

be summarized as an optimization process, specifically an optimization aiming to find the minima of a quantity that depends parametrically on the parameters of an auxiliary function. For ML, the quantity being minimized is the loss function, while for VM is the expectation value of the Hamiltonian. The auxiliary function is the ANNs for ML, while for VM is the trial wave function. As a consequence, the parameters of the auxiliary function are the weights and biases for ML and the variational parameters for VM. While the aim of ML is to correctly predict a value that represent performing a task, VM aim is to correctly predict GS properties. Therefore, the ANVMC method explores this equivalence between the two methods and interpret the minimization of the energy as the training process from ML.

IV. EXAMPLES

The simulations in this tutorial were performed using the program Artificial Neural Network-based Variational Monte Carlo Introduction (ANVMC-intro) [57] available on GitHub. Additionally, pseudo algorithms based on the Section III are described on the Section C, which can serve as reference for beginners. Each simulation considered $M = 4096$ samples per step and, a total of $N_{\text{OI}} = 5000$ optimization iterations. The employed ANN architecture is composed by $L = 4$ layers, where the layers [1, 2, 3, 4] were formed by [24, 32, 16, 1] neurons, respectively. This architecture is broadly applied in this work, unless otherwise stated. The program performed all simulations using a single NVIDIA RTX A5500.

A. Harmonic oscillator

As one of the simplest and solvable systems, a particle in a one dimensional harmonic oscillator is one of the best proving grounds for testing the ANN based trial wave functions. For examples like this that are described in terms of only one variable, that is, $N = 1$ and $D = 1$, the system component is written as $x \equiv \mathbf{x}$. Considering a particle of mass m and a confinement frequency of ω ,

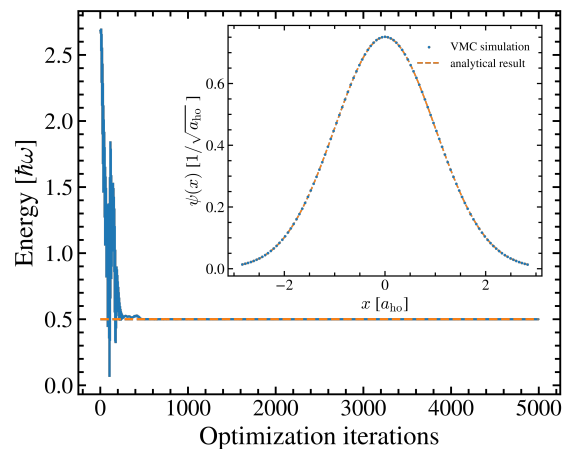


FIG. 3. Minimization process for the harmonic oscillator potential showing the energy evolution as a function of the iterations. The inset presents the analytical ground state and optimized trial state.

the potential $V(x)$ reads

$$V(x) = \frac{m\omega^2 x^2}{2}. \quad (8)$$

Choosing $\hbar\omega$ as the energy units and $a_{\text{ho}} = \sqrt{\hbar/m\omega}$ as length units, the exact GS energy is $E_0 = 1/2$ and the dimensionless wave function is given by $\psi(\hat{x}) = \pi^{-1/4} \exp(-\hat{x}^2/2)$.

A comparison between exact solutions and the results of the Monte Carlo simulation for the harmonic oscillator are displayed in Fig. 3. Initially, the M samples are drawn from a uniform distribution centred at the origin. Results obtained in this work are shown in blue dots and analytical results in dashed orange lines. The main graph shows the evolution of the energy as function of the optimization iterations, where the error bars are also included. The energy quickly reaches the GS energy as the simulation evolves. Moreover, the inset compares the trial wave function after the optimization procedure with the exact solution. For that, it was necessary to estimate the normalization factor \mathcal{N} through a numerical quadrature integration. Notably, the optimized ANN shows excellent agreement with the exact solution.

B. Morse oscillator

This interatomic potential is often used to describe interactions between atoms, since the vibrational structure of molecules can be better approximated by the Morse oscillator than the harmonic oscillator. This is mainly due to the fact that this potential has unbound states and is anharmonic. Therefore, it also can describe bond breaking and account for the imbalance present in bonds. The potential is defined as

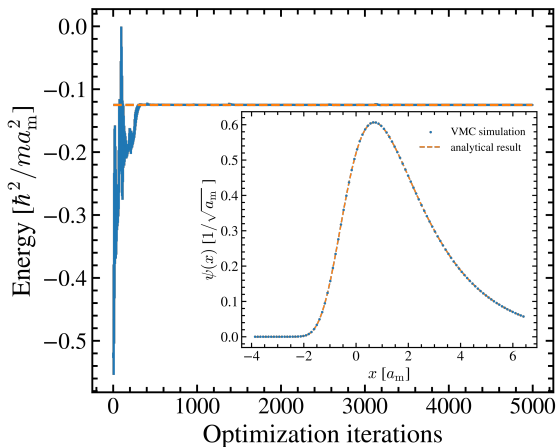


FIG. 4. Minimization process for the Morse oscillator. The main graph shows the energy progression as a function of the number of iterations. The inset presents the analytical ground state and optimized trial state.

$$V(x) = D (e^{-2ax} - 2 e^{-ax}) , \quad (9)$$

where the natural length scale is $a_m = 1/a$, which implies that the energy units are given by \hbar^2/ma_m^2 . The well depth of the potential is considered to be $D = 1/2$ for simplicity. In this units, the analytical GS energy is $E_0 = -1/8$ and the dimensionless wave function is given by $\psi(\hat{x}) = \sqrt{2} \exp[-e^{-\hat{x}} - \hat{x}/2]$.

The results for ANN-based trial wave function description of the Morse oscillator are presented in Fig. 4. The optimization procedure presents the system energy converging towards the GS energy $E_0 = -0.125$, while the inset displays a comparison between the analytical and optimized trial wave functions, which shows excellent agreement. This result already hints on the versatility of ANNs as trial wave functions. With exactly the same parametrized class of functions ϕ_θ , accurate results were obtained for systems described by reasonably different potentials.

C. Poschl-Teller potential

To demonstrate this versatility even further, consider a class of potentials that are exactly solvable, smooth, and supports a tunable number of bound states given by the Poschl-Teller potential described by the form

$$V(x) = -\frac{\hbar^2 \lambda(\lambda + 1)}{2ma_{pt}^2} \operatorname{sech}^2\left(\frac{x}{a_{pt}}\right) , \quad (10)$$

where a_{pt} is the natural length scale and, consequently, the energy units are given by \hbar^2/ma_{pt}^2 . The free parameter λ controls the number of bound states. For the performed simulation it was considered only one bound state $\lambda = 1$

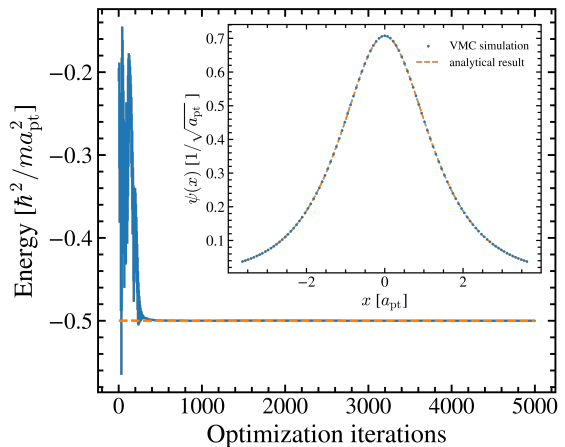


FIG. 5. Minimization process for the Poschl-Teller potential. The main figure shows energy values as a function of optimization iterations. The inset presents the analytical ground state and optimized trial state.

and, therefore, the dimensionless GS energy is $E_0 = -1/2$ and the analytical GS wave function is $\psi(\hat{x}) = \operatorname{sech}(\hat{x})$.

This potential is often used in the context of atoms, molecules, and optics (AMO) physics, since it closely resembles realistic optical and trapping potentials, therefore, making it ideal for benchmarking. Once again, the evolution of the variational energy and its standard error as a function of the number of optimization steps is displayed in Fig. 5, while the inset represents the comparison between analytical and optimized trial wave functions. The agreement among simulation and exact results is clear.

Hence, the ANN trial wave function was capable of accurately describing one-dimensional integrable systems. The next examples shall investigate systems with higher dimensions, particularly, all following examples will consider $D = 3$. For single particle systems, that is $N = 1$, the components are written as $\mathbf{x} \equiv \mathbf{r} = \{x, y, z\}$, while for two particle systems $\mathbf{x} \equiv \{\mathbf{r}_1, \mathbf{r}_2\}$, where $\mathbf{r}_i = \{x_i, y_i, z_i\}$.

D. Yukawa potential

The description of nuclear forces by the Yukawa potential helped to understand the concept of forces mediated by massive fields and to explain the finite range aspect of nuclear forces. Beyond its original purpose, other examples of applications for this potential include the screening Coulomb interactions in solids and effective models in ultracold atomic systems. Recently, analytical solutions based on super-potentials were proposed [58], although only Taylor expansions of the solution can be computed. The Yukawa potential is

$$V(\mathbf{r}) = -\alpha \frac{e^{-r/d}}{r} , \quad (11)$$

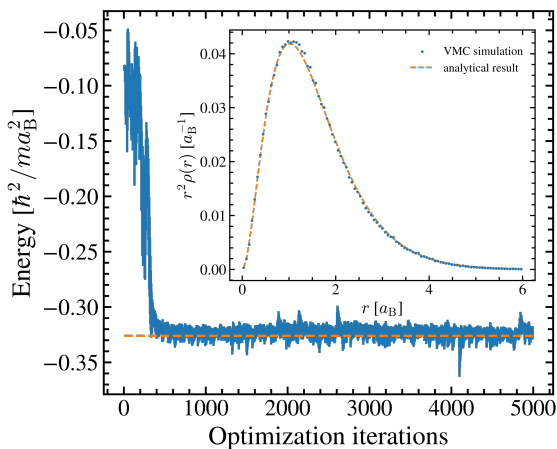


FIG. 6. ANN-based trial state description of the Yukawa potential. The main graph displays the energy as a function of the optimization iterations, while the inset compares the radial PDF sampled in the simulation with the analytical PDF up to order δ^3 .

where d is a potential parameter and the particle distance is $r = |\mathbf{r}|$. Considering a particle of mass m and length units given by the Bohr radius $a_B = \hbar/mc\alpha$, where α is the fine-structure constant and c is the speed of light, the energy units are defined as Hartree \hbar^2/ma_B^2 . Expanding the analytical solution to order δ^3 , where $\delta = a_B/d$, the GS wave function reads $\psi(\hat{r}) \propto e^{-r + \frac{1}{12}\delta^2(3-2\delta)r^2 - \frac{\delta^3}{18}r^3}$, while the dimensionless GS energy is $-1/2(1 - 2\delta + 3\delta^2/2 - \delta^3)$. This expansion is reasonable for $\delta = 0.2$ or smaller values and, therefore, that is the value considered in the simulation.

The variational energy of the ANN trial state during the optimization procedure is shown in Fig. 6. The energy quickly converges to the analytical result and oscillates around it. Furthermore, a comparison between the analytical radial PDF and the stochastic sampled PDF are presented in the inset, demonstrating an excellent agreement.

E. Hydrogen molecular ion

As a more realistic example, consider the hydrogen molecular ion H_2^+ , which is stabilized by a moving electron on the static field of two protons in their equilibrium positions, separated by $R = 2.004 a_B$. In chemistry, considering the protons of a molecule as static charges is known as the Born-Oppenheimer approximation, which approximates the kinetic energies of the protons to zero, since they are much heavier than electrons. Therefore, the potential energy is expressed as

$$V(\mathbf{x}) = -\frac{e^2/4\pi\epsilon_0}{|\mathbf{r} - \mathbf{R}/2|} - \frac{e^2/4\pi\epsilon_0}{|\mathbf{r} + \mathbf{R}/2|} + \frac{e^2/4\pi\epsilon_0}{R}, \quad (12)$$

where e is the fundamental charge, ϵ_0 is the permittivity

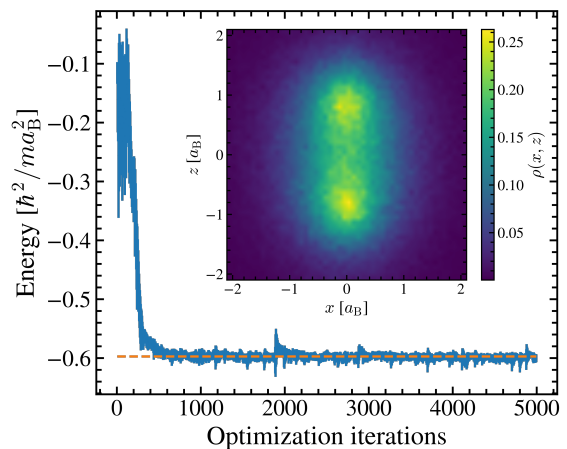


FIG. 7. Description of H_2^+ by ANN-based trial functions. The minimization process is showing the evolution of the energy as a function of the number of iterations. The inset present a 2D projected distribution function.

of vacuum, and $\mathbf{R} = R \hat{z}$ is the vector that connects the two protons. For this and the final example, consider the system in atomic units, that is, Bohr radius as length scale and Hartree as energy units.

The solutions of this system are not analytically known, while numerical solutions predict that the GS energy is -0.59724 Hartree [59]. The simulation results for the evolution of the energy during the minimization process are displayed in Fig. 7 and compared with numerical results. Additionally, the inset shows the xz projected PDF $\rho(x, z) = \int dy |\psi_\theta(\mathbf{r})|^2$, which demonstrate the larger bond due to the absence of one electron. Even without the information of the proton positions, the ANN was able to learn the GS function.

F. Hydrogen molecule

Lastly, the hydrogen molecule H_2 was studied. Once again the protons are considered static in their equilibrium position and separated by $R = 1.399 a_0$. The resulting Schrodinger equation describe the behaviour of the $N = 2$ electrons and, therefore, the total potential of the system is written as

$$V(\mathbf{x}) = \frac{e^2}{4\pi\epsilon_0} \left[-\frac{1}{|\mathbf{r}_1 - \mathbf{R}/2|} - \frac{1}{|\mathbf{r}_1 + \mathbf{R}/2|} - \frac{1}{|\mathbf{r}_2 - \mathbf{R}/2|} - \frac{1}{|\mathbf{r}_2 + \mathbf{R}/2|} + \frac{1}{|\mathbf{r}_1 - \mathbf{r}_2|} + \frac{1}{R} \right], \quad (13)$$

where $\mathbf{R} = R \hat{z}$ is the vector that connects the two protons. In order to reach GS level accuracy, the ANN architecture employed was enlarged, making use of [64, 64, 64, 1] neurons for each respective layer. Moreover, the system is formed by two fermions and, hence, it requires the wave function to be antisymmetric. For

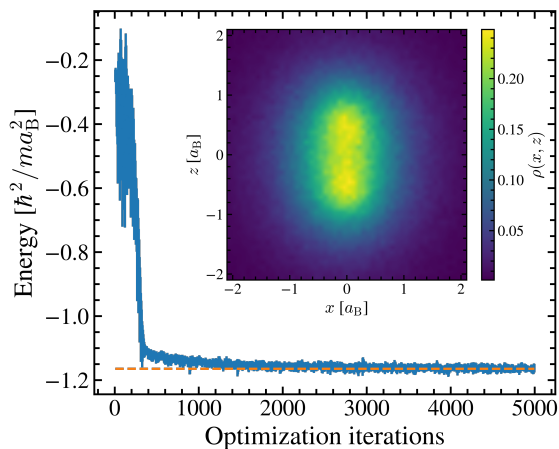


FIG. 8. The minimization process for the H_2 shows the energy as a function of optimization iterations. The inset present a 2D projected distribution function.

the GS, the system is in a singlet spin state, which is antisymmetric. Accordingly, the spatial wave function must be symmetric. Nevertheless, that property is not imposed to the ANN trial state. Instead, the training process is responsible to learn this feature.

In this scenario, the numerical available energy result predicts -1.1645 Hartree for the GS energy [59]. The progression of the variational energy as a function of the number of optimization iterations is displayed in Fig. 8. Initially, the procedure shows a quick reduction on the energy estimation followed by a slow decay towards the reference energy. By the end of the procedure, the energy is oscillating around the predicted value. Additionally, the projected PDF is also shown in the inset.

Therefore, quantitative results across all studied systems are summarized on Table I, where the energies are shown together with their respective statistical errors. The table also shows the reference energies that each system was compared to. The accuracy achieved by the ANN trial states is remarkable, which reinforces the large versatility within a single parametrized function. It is also important to point out that this architecture does not implement any physical feature other than granting a finite normalization of the trial state. By naively offering $\{q_1, \dots, q_{ND}\}$ all component coordinates as an input for the ANN, properties such as cusp conditions and spin symmetry have to be learned by the ANN. Even without these features built in the architecture, the learning process was able to capture the GS accurately.

V. FINAL REMARKS

This tutorial presented a systematic application across distinct physical systems of the ANNVMC method in a introductory manner. By explaining separately the regression problem in ML and the VMC method, then tracing connections among the components of each one,

TABLE I. Comparison between the optimized (columns two and five) and reference (columns three and six) energy values across the studied systems (columns one and four).

System	ANN-VMC	Ref.	System	ANN-VMC	Ref.
E_{HO}	0.5000(1)	0.5	E_{Y_u}	-0.322(5)	-0.326
E_{MO}	-0.12500(2)	-0.125	$E_{H_2^+}$	-0.595(5)	-0.59724
E_{PT}	-0.50001(5)	-0.5	E_{H_2}	-1.16(1)	-1.1645

the theory behind ANNVMC was carefully uncovered. Moreover, pseudo algorithms were proposed to support the application of the method by beginners, as well as the availability of the program used to perform the simulations. Employing this open source code developed by the author, systems of pedagogical interest were studied and the GS of them were described by the optimized ANNs trial states.

The ANN based trial states, as proposed in this work, are quite limited. Due to the simplicity and lack of physical insights of the Ansatz, high accurate results are restricted by the number of degrees of freedom, that is, $n_0 = ND$. Considering that the particles interact, as n_0 grows, the ANN size needed to reach GS accuracy also grows, as well as the need to perform more optimization steps. In principle, because of the Cybenko theorem [11], an infinitely large ANN can capture the GS wave function of any system regardless of the simplicity of the trial state. However, that is limited due to computer power and simulation time. Therefore, there is a necessity of going beyond the simplest ANN architecture for more complex systems.

Furthermore, depending on the system, symmetries, such as global translation invariance, can even make the training unfeasible if the trial state is built without considering this property [20]. Other examples [4, 22, 60] of properties that can be added to significantly improve the training of ANNs include spin statistics, cusp conditions, periodicity, backflow and equivariant transformations. Overly distinct system properties requires tweaks in the architecture and input features that are provided to the ANN. However, class of systems with similar properties can be described by the same architecture, even though they can be intrinsically distinct. For example, electronic structure of circular quantum dots [61] and Bicyclobutane molecule [5] use the same architecture because they belong to the same class of systems, that is, finite size spin $1/2$ fermions. Despite system dependent adjustments being required sometimes, the general structure of stacking layers of artificial neurons is preserved and employed across different applications successfully.

Finally, ANNs based trial wave functions have been proving to be able to describe quantum states across several systems with distinct features. The flexibility, performance and the generalization character of such trial functions show how powerful is this tool and it demonstrate that they can aid the development of physics re-

search. Nevertheless, there are other approaches and methods that also employ concepts borrowed from the AI field to study physics. For example, one perspective would be to study ultracold molecules by means of

Gross–Pitaevskii equation associated with ANNs.

Acknowledgments: The author thanks Prof. Rost for fruitful discussions.

The authors have no conflicts to disclose.

-
- [1] M. Ntampaka, H. Trac, D. J. Sutherland, N. Battaglia, B. Póczos, and J. Schneider, *The Astrophysical Journal* **803**, 50 (2015).
- [2] D. Guest, K. Cranmer, and D. Whiteson, *Annual Review of Nuclear and Particle Science* **68**, 161 (2018).
- [3] D.-L. Deng, X. Li, and S. Das Sarma, *Phys. Rev. X* **7**, 021021 (2017).
- [4] D. Pfau, J. S. Spencer, A. G. D. G. Matthews, and W. M. C. Foulkes, *Phys. Rev. Res.* **2**, 033429 (2020).
- [5] J. S. Spencer, D. Pfau, A. Botev, and W. M. C. Foulkes, “Better, faster fermionic neural networks,” (2020), arXiv:2011.07125 [physics.comp-ph].
- [6] D. Wu, L. Wang, and P. Zhang, *Phys. Rev. Lett.* **122**, 080602 (2019).
- [7] T. Wen, L. Zhang, H. Wang, W. E, and D. J. Srolovitz, *Materials Futures* **1**, 022601 (2022).
- [8] J. Bardeen, L. N. Cooper, and J. R. Schrieffer, *Phys. Rev.* **108**, 1175 (1957).
- [9] P. Anderson, *Materials Research Bulletin* **8**, 153 (1973).
- [10] R. B. Laughlin, *Phys. Rev. Lett.* **50**, 1395 (1983).
- [11] G. Cybenko, *Mathematics of Control, Signals and Systems* **2**, 303 (1989).
- [12] A. Nagy and V. Savona, *Physical Review Letters* **122**, 250501 (2019).
- [13] C. Roth, A. Szabó, and A. H. MacDonald, *Physical Review B* **108**, 054410 (2023).
- [14] L. Yang, Z. Leng, G. Yu, A. Patel, W.-J. Hu, and H. Pu, *Physical Review Research* **2**, 012039 (2020).
- [15] Y. Qian, W. Fu, W. Ren, and J. Chen, *The Journal of Chemical Physics* **157**, 164104 (2022).
- [16] D. Pfau, S. Axelrod, H. Sutterud, I. von Glehn, and J. S. Spencer, *Science* **385**, eadn0137 (2024), publisher: American Association for the Advancement of Science.
- [17] G. Pescia, J. Nys, J. Kim, A. Lovato, and G. Carleo, *Phys. Rev. B* **110**, 035108 (2024), publisher: American Physical Society.
- [18] G. Cassella, H. Sutterud, S. Azadi, N. Drummond, D. Pfau, J. S. Spencer, and W. Foulkes, *Phys. Rev. Lett.* **130**, 036401 (2023), publisher: American Physical Society.
- [19] W. T. Lou, H. Sutterud, G. Cassella, W. Foulkes, J. Knolle, D. Pfau, and J. S. Spencer, *Phys. Rev. X* **14**, 021030 (2024), publisher: American Physical Society.
- [20] W. Freitas and S. A. Vitiello, *Quantum* **7**, 1209 (2023).
- [21] W. Freitas, B. Abreu, and S. A. Vitiello, *Journal of Low Temperature Physics* (2024), 10.1007/s10909-024-03061-w.
- [22] G. Pescia, J. Han, A. Lovato, J. Lu, and G. Carleo, *Phys. Rev. Research* **4**, 023138 (2022).
- [23] H. H. Goldstine, *The computer from Pascal to von Neumann* (Princeton University Press, 1993).
- [24] A. A. Lovelace, *Taylor’s Scientific Memoirs* **3**, 666 (1842).
- [25] G. Welchman, *The Hut Six Story: Breaking the Enigma Codes* (McGraw-Hill, 1982).
- [26] B. RANDELL, in *A History of Computing in the Twentieth Century*, edited by N. METROPOLIS, J. HOWLETT, and G.-C. ROTA (Academic Press, San Diego, 1980) pp. 47–92.
- [27] H. H. Goldstine and A. Goldstine, in *The Origins of Digital Computers: Selected Papers* (Springer, 1946) pp. 359–373.
- [28] J. Von Neumann, *IEEE Annals of the History of Computing* **15**, 27 (1993).
- [29] A. M. TURING, *Mind* **LIX**, 433 (1950), <https://academic.oup.com/mind/article-pdf/LIX/236/433/30123314/lix-236-433.pdf>.
- [30] S. Bubeck, C. Coester, R. Eldan, T. Gowers, Y. T. Lee, A. Lupsasca, M. Sawhney, R. Scherrer, M. Sellke, B. K. Spears, D. Unutmaz, K. Weil, S. Yin, and N. Zhivotovskiy, “Early science acceleration experiments with gpt-5,” (2025), arXiv:2511.16072 [cs.CL].
- [31] DeepSeek-AI, “Deepseek-v3 technical report,” (2025), arXiv:2412.19437 [cs.CL].
- [32] A. Uchendu, Z. Ma, T. Le, R. Zhang, and D. Lee, *CoRR abs/2109.13296* (2021).
- [33] S. Dargan, S. Bansal, M. Kumar, A. Mittal, and K. Kumar, *ARCHIVES OF COMPUTATIONAL METHODS IN ENGINEERING* **30**, 1057 (2023).
- [34] Z. Wang, J. Zhan, C. Duan, X. Guan, P. Lu, and K. Yang, *IEEE TRANSACTIONS ON NEURAL NETWORKS AND LEARNING SYSTEMS* **34**, 3811 (2023).
- [35] U. Raucci, A. Valentini, E. Pieri, H. Weir, S. Seritan, and T. J. Martinez, *NATURE COMPUTATIONAL SCIENCE* **1**, 42 (2021).
- [36] L. Li, B. Lei, and C. Mao, *JOURNAL OF INDUSTRIAL INFORMATION INTEGRATION* **26** (2022).
- [37] G. Moore, *PROCEEDINGS OF THE IEEE* **86**, 82 (1998).
- [38] M. Roser, H. Ritchie, and E. Mathieu, *Our World in Data* (2023), <https://ourworldindata.org/moores-law>.
- [39] I. Goodfellow, Y. Bengio, and A. Courville, *Deep learning* (MIT press, 2016).
- [40] W. S. McCulloch and W. Pitts, *The bulletin of mathematical biophysics* **5**, 115 (1943).
- [41] F. Rosenblatt, *Psychological review* **65**, 386 (1958).
- [42] K. Fukushima, *Biological Cybernetics* **20**, 121 (1975).
- [43] D. E. Rumelhart, J. L. McClelland, and P. R. Group, *Parallel Distributed Processing, Volume 1: Explorations in the Microstructure of Cognition: Foundations* (The MIT Press, 1986).
- [44] D. E. Rumelhart, G. E. Hinton, and R. J. Williams, *Nature* **323**, 533 (1986).
- [45] G. E. Hinton, *Progress in brain research* **165**, 535 (2007).
- [46] Y. LeCun, Y. Bengio, *et al.*, *Large-scale kernel machines* **5**, 127 (2007).
- [47] J. Carrasquilla and R. G. Melko, *Nature Physics* **13**, 431 (2017).
- [48] G. Carleo, I. Cirac, K. Cranmer, L. Daudet, M. Schuld, N. Tishby, L. Vogt-Maranto, and L. Zdeborová, *Rev. Mod. Phys.* **91**, 045002 (2019).

- [49] G. Györgyi, Phys. Rev. A **41**, 7097 (1990).
- [50] J. Albert and R. H. Swendsen, Physics Procedia **57**, 99 (2014), proceedings of the 27th Workshop on Computer Simulation Studies in Condensed Matter Physics (CSP2014).
- [51] C. Cohen-Tannoudji, B. Diu, F. Laloe, and B. Dui, *Quantum Mechanics (2 vol. set)* (Wiley-Interscience, 2006).
- [52] N. Metropolis, A. W. Rosenbluth, M. N. Rosenbluth, A. H. Teller, and E. Teller, The Journal of Chemical Physics **21**, 1087 (1953).
- [53] M. Mascagni and A. Srinivasan, ACM Trans. Math. Softw. **26**, 436–461 (2000).
- [54] J. Bradbury, R. Frostig, P. Hawkins, M. J. Johnson, C. Leary, D. Maclaurin, G. Necula, A. Paszke, J. VanderPlas, S. Wanderman-Milne, and Q. Zhang, “JAX: composable transformations of Python+NumPy programs,” (2018).
- [55] T. Mitchell, Publisher: McGraw Hill (1997).
- [56] D. P. Kingma and J. Ba, “Adam: A method for stochastic optimization,” (2017), arXiv:1412.6980 [cs.LG].
- [57] W. Freitas, “Artificial Neural Network-based Variational Monte Carlo Introduction,” (2025).
- [58] M. Napsuciale and S. Rodríguez, Physics Letters B **816**, 136218 (2021).
- [59] I. Kosztin, B. Faber, and K. Schulten, American Journal of Physics **64**, 633 (1996).
- [60] M. Ruggeri, S. Moroni, and M. Holzmann, Phys. Rev. Lett. **120**, 205302 (2018).
- [61] W. Freitas, B. Abreu, and S. A. Vitiello, Phys. Rev. B **112**, 165109 (2025).

Appendix A: Blocking method and standard error estimation

Since the Monte Carlo integration is based on a Markov chain, successive samples are correlated. Therefore, the effective number of samples is smaller than the actual number of samples M . Consequently, the usual standard error estimation is too optimistic. To illustrate the procedure, consider a series of data E_1, E_2, \dots, E_M . The blocking procedure consists on grouping the data in blocks of size b and computing their averages,

$$\bar{E}_k^{(b)} = \frac{1}{b} \sum_{i=(k-1)b+1}^{kb} E_i. \quad (\text{A1})$$

The variance of the blocked-averaged data is also computed through

$$\sigma_b^2 = \frac{1}{M-1} \sum_i^{M/b} \left(\bar{E}_i^{(b)} - \bar{E} \right)^2, \quad (\text{A2})$$

where the total average data \bar{E} is computed over all data set, namely, $\bar{E} = \sum_i^M E_i/M$. Finally, the standard error of the mean is given by

$$\text{SEM} = \sqrt{\frac{\sigma_b^2}{M}}. \quad (\text{A3})$$

For small block sizes b , the SEM is underestimated. As the block size is gradually increased, eventually, the error saturates and start fluctuating around a constant value. In this later stage, the blocks are large enough to make the blocked-averaged data $\bar{E}_i^{(b)}$ to be effectively independent. As a consequence, the correct error estimation is given in this length range of block sizes.

Appendix B: Adaptive Moment Estimation optimizer

When dealing with noisy gradients coming from stochastic methods and loss landscapes in high dimensional spaces, naive gradient-based optimization methods are likely to perform poorly. The adaptive moment estimation [56] is a popular optimization algorithm used in machine learning in order to overcome the mentioned limitations of simple gradient descent methods. The algorithm employs weighted moving averages to estimate first and second moments of the loss gradient, which are used in the update of the model parameters. The procedure aids in the control of the step length individually for each parameter and address convergence issues.

Denoting the loss gradient with respect to the parameters as $g_t = \nabla \mathcal{L}[\theta_t]$, the algorithm updates iteratively state variables p_t and q_t according to the following equations:

$$p_t = \beta_1 p_{t-1} + (1 - \beta_1) g_t, \quad (\text{B1a})$$

$$q_t = \beta_1 q_{t-1} + (1 - \beta_2) g_t^2, \quad (\text{B1b})$$

$$\hat{p}_t = \frac{p_t}{1 - \beta_1}, \quad (\text{B1c})$$

$$\hat{q}_t = \frac{q_t}{1 - \beta_2}, \quad (\text{B1d})$$

where $p_0 = q_0 = 0$ and the hyperparameters η , β_1 , β_2 , and ϵ controls the performance of the algorithm. Typical values are $\eta = 10^{-3}$, $\beta_1 = 0.9$, $\beta_2 = 0.999$, and $\epsilon = 10^{-8}$. Furthermore, the proposed update for the parameters is written as:

$$\Delta \theta_t = -\frac{\eta \hat{p}_t}{\sqrt{\hat{q}_t + \epsilon}}. \quad (\text{B2})$$

Therefore, the parameters are updated according to $\theta_{t+1} = \theta_t + \Delta \theta_t$. Additionally, the learning rate η can also be adapted as a function of t , granting that the steps become smaller as the optimization steps t increase. One example of such learning rate schedule would be

Algorithm1 ANN algorithm

Require: Network architecture $\text{NetArch} \leftarrow \{n_\ell\}_{\ell=0}^L$

- 1: **procedure** INITIALIZEWNB(NetArch)
- 2: $\mathbf{W}_\ell \leftarrow \text{RandN}(n_\ell, n_{\ell-1})/\sqrt{n_{\ell-1}}$ for $\ell = 1, \dots, L$
- 3: $\mathbf{b}_\ell \leftarrow \text{RandN}(n_\ell)$ for $\ell = 1, \dots, L$
- 4: $\theta \leftarrow \{\mathbf{W}_\ell, \mathbf{b}_\ell\}_{\ell=1}^L$ **return** θ
- 5: **end procedure**

Require: Input vector $\mathbf{x} \in \mathbb{R}^{n_0}$ and model parameters θ

- 6: **procedure** FFNN(\mathbf{x}, θ)
- 7: $\mathbf{h}_0 \leftarrow \mathbf{x}$
- 8: **for** $\ell = 1$ to $L - 1$ **do**
- 9: $\mathbf{z}_\ell \leftarrow \text{matmul}(\mathbf{W}_\ell, \mathbf{h}_{\ell-1}) + \mathbf{b}_\ell$
- 10: $\mathbf{h}_\ell \leftarrow \tanh(\mathbf{z}_\ell)$
- 11: **end for**
- 12: $\mathbf{z}_L \leftarrow \text{matmul}(\mathbf{W}_L, \mathbf{h}_{L-1}) + \mathbf{b}_L$
- 13: $\mathbf{y} \leftarrow -\ln(1 + e^{\mathbf{z}_L})$ **return** $\sum_i y_i$
- 14: **end procedure**

Algorithm2 NN-VMC algorithm

Require: θ

- 1: $\mathbf{x}_0 \leftarrow \text{RandU}(n_0)$
- 2: **for** $i \leftarrow 1$ to N_{OI} **do**
- 3: **for** $j \leftarrow 1$ to M **do**
- 4: $\xi \leftarrow \text{RandU}(n_0)$
- 5: $\mathbf{x}_t \leftarrow \mathbf{x}_j + \Delta^{1/2}(\xi - \mathbf{x}_j)$
- 6: $q \leftarrow p(\mathbf{x}_t)/p(\mathbf{x}_j)$
- 7: $\xi' \leftarrow \text{RandU}(1)$
- 8: **if** $q > \xi'$ **then**
- 9: $\mathbf{x}_j \leftarrow \mathbf{x}_t$
- 10: **end if**
- 11: $E_j \leftarrow E_L(\mathbf{x}_j)$
- 12: $g_{j,\theta} \leftarrow 2\nabla_\theta \ln |\psi_\theta(\mathbf{x}_j)|$
- 13: **end for**
- 14: $E_{\text{VMC}} \leftarrow \langle E_j \rangle_{j=1}^M$
- 15: $\Delta E_{\text{VMC}} \leftarrow \text{SEM}[E_j]$
- 16: $G_\theta \leftarrow \langle (E_j - E_{\text{VMC}}) g_{j,\theta} \rangle_{j=1}^M$
- 17: $\Delta\theta \leftarrow \text{ADAM}[G_\theta]$
- 18: $\theta \leftarrow \theta + \Delta\theta$
- 19: **end for**

$$\eta(t) = \frac{\eta_0}{(1 + t/a_{\text{delay}})^{a_{\text{decay}}}} \quad (\text{B3})$$

where η_0 is the initial learning rate, a_{delay} controls from which step the suppression of the learning rate will start, and a_{decay} controls how fast is the decay.

Appendix C: ANN and VMC algorithms

Here is presented two pseudo codes that show the implementation details of the ANN algorithm and the VMC algorithm. The functions $\text{RandU}(\cdot)$ and $\text{RandN}(\cdot)$ are supposed to be pseudo random number generators for the uniform and normal distribution, respectively. The expected input is the length of the dimensions of the array to be generated, that is, the size of the array if it is a vector or the number of rows and columns if it is a matrix.

Denoting the number of degrees of freedom, that is, number of particles multiplied by the number of spatial dimensions as $n_0 = ND$ and the width of each ANN layer by the set $\{n_\ell\}_{\ell=0}^L$, the Algorithm 1 presents two procedures, namely, functions that define how to initialize the weights and biases (InitializeWnB) and how to compute the ANN output (FFNN).

On the other hand, the implementation of the optimization procedure is presented in Algorithm 2. The user defined parameters are the number of optimization iterations denoted by N_{OI} , and the batch size (or number of walkers) denoted by M . Usually, the quantum Monte Carlo codes are written in the logarithm domain in order to avoid loss of numerical precision. Note that, however, the pseudo code is not taking that detail into account, although the available code [57] does that. Therefore, for more details, the reader is encouraged to look carefully into the code employed in the simulations.